Double and Single Network Phases in Polystyrene-block-poly(L-lactide) Diblock Copolymers

4 **AUTHORS**, INCLUDING:

Han-Yu Hsueh
University of Massachusetts Amherst

15 PUBLICATIONS **232** CITATIONS

Double and Single Network Phases in Polystyrene-*block*-poly(L-lactide) Diblock Copolymers

Xin-Bo Wang,[†,‡] Ting-Ya Lo,[†] Han-Yu Hsueh,[†] and Rong-Ming Ho*,[†]

[†]Department of Chemical Engineering, National Tsing Hua University, Hsinchu 30013, Taiwan

[‡]School of Materials Science and Engineering, Harbin Institute of Technology at Weihai, Weihai, Shandong 264209, China

ABSTRACT: Here, the phase behaviors of polystyrene-*block*-poly(L-lactide) (PS−PLLA) diblock copolymers are studied, and network phases can be found. In addition to conventional double gyroid phase with double networks, a single network phase (an *Fddd* phase with orthorhombic network) can be found, as evidenced by small-angle X-ray scattering and transmission electron microscopy (TEM). The single network texture with trivalent connectors of the *Fddd* can be directly visualized by using 3D TEM (i.e., electron tomography), and the observation under polarized light microscopy shows its birefringence character. The formation of stable *Fddd* is attributed to intrinsic inhomogeneity in the chain conformations of the chiral block (i.e., PLLA). Subsequently, nanoporous PS with continuous nanochannel networks can be obtained by hydrolysis of the PLLA block in the PS−PLLA and then used as a template for sol−gel reaction of tetraethyl orthosilicate. Consequently, nanoporous SiO$_2$ with free-standing, well-defined network texture can be fabricated after removal of the PS template to give an open-cell porous ceramic material with high specific surface area (as high as 1170 m^2/g) due to its nanostructured texture and high porosity.
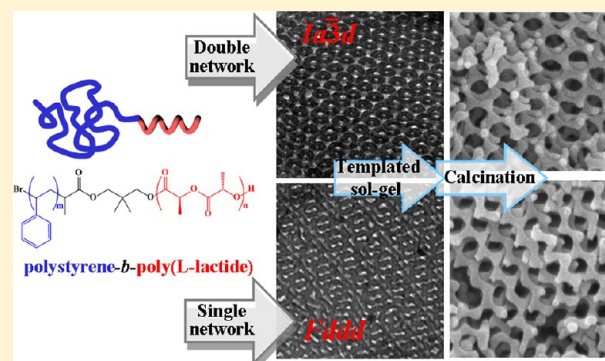
INTRODUCTION

Block copolymers (BCPs) are composed of different blocks of polymerized monomers connected with chemical bonding and can form various nanostructured phases due to microphase separation.[1] Free energy minimization drives BCPs to adopt periodically ordered morphologies, and a balance of interfacial tension and entropic stretching energy considerations governs selection of the equilibrium state.[2] Among those nanostructured phases, network phases always receive intensive attention because of their unique three-dimensional continuous texture. Those networks have continuous space structure which can be characterized by translational symmetry in three dimensions and divide space into independent, intertwining microdomains. Materials with network texture have captivated researchers because of their superior mechanical properties and could potentially be applied in technologies such as catalysis,[3] separations,[4] nanoreactor,[5−7] and photoelectric device.[8−10] Network phases formed by the self-assembly of diblock copolymers include double gyroid (DG) (Q^{230}),[11−13] ordered bicontinuous double diamond (OBDD) (Q^{224}),[14,15] and orthorhombic *Fddd* network (O^{70}).[16−19] The network structures found in the self-assembly of block copolymers have been considered as cubic structure until Bates and co-workers found *Fddd* in polyisoprene-*b*-polystyrene-*b*-poly-(ethylene oxide) (ISO) triblock terpolymers which was identified as a noncubic structure.[20] They proved network skeleton of the *Fddd* phase consists of continuous minor-block microdomain connected with trivalent connector. Also, the

Fddd phase from the self-assembly of triblock terpolymers was theoretically predicted by Tyler and Morse[16] and later experimentally observed.[17] The *Fddd* phase is often found during the phase transition process[17−19] and also found in diblock melts within a narrow region that overlaps the weak segregation end of the gyroid region.[16] Yamada and co-workers proposed a two-mode expansion method in the weak segregation regime and demonstrated that there truly exists a stable *Fddd* phase.[21] Morse and co-workers studied the phase diagram of weakly segregated diblock copolymer using a straightforward extension of Leibler's theory[22] and found that the *Fddd* network has a ratio of unit cell parameters (a:b:c = 1:2:2$\sqrt{3}$). Experimentally, Takenaka and co-workers reported that *Fddd* phase exists as a stable phase in polystyrene-*block*-polyisoprene (PS−PI) diblock copolymers between lamellar (L) and DG phases with $\chi N < 50$.[17]

A few years ago, BCPs comprising chiral entities, denoted as chiral BCPs (BCPs*), were designed to fabricate helical architectures from self-assembly.[23,24] A helical phase (denoted H* to distinguish its *P*622 symmetry from that of the normal hexagonally packed cylinder phase (HC) with *P*6*mm* symmetry) in addition to sphere (S), HC, DG, and L was discovered in the self-assembly of polystyrene-*b*-poly(L-lactide) (PS−PLLA) BCPs*.[25−27] Moreover, thermal annealing treat-

ment will induce a phase transition from H* to DG, suggesting that the H* phase is a long-lived metastable phase.[26] In this study, we aim to systematically examine the phase behavior of the PS–PLLA, in particular with the volume fraction of PLLA ranging from 0.33 to 0.37 at which stable network phases are expected to be found. Interestingly, in contrast to conventional DG with double networks, a single network phase (an *Fddd* phase with orthorhombic network) can be found, as evidenced by small-angle X-ray scattering (SAXS) and transmission electron microscopy (TEM). The single network texture with trivalent connectors of the *Fddd* is directly visualized by using 3D TEM (i.e., electron tomography), and the observations under polarized light microscopy (PLM) show significant birefringence character due to the anisotropic property of the orthorhombic structure. Nanoporous PS with a continuous nanochannel network can be obtained by hydrolysis of the PLLA blocks in the PS–PLLA and then used as a template for sol–gel reaction of tetraethyl orthosilicate (TEOS). Consequently, after removal of the PS template, nanoporous SiO_2 with free-standing, well-defined single network texture and open-cell character can be fabricated for the first time, as evidenced by field emission scanning electron microscopy (FESEM) observations. The specific surface area of this open-cell porous inorganic material can reach 1170 m^2/g due to its nanostructured texture and high porosity.

■ EXPERIMENTAL SECTION

Synthesis of PS–PLLA Block Copolymers. The PS–PLLA diblock coplymers were prepared by two living polymerization processes which have been described in our previously published results.[25,27] The number-average molecular weight and polydispersity index (PDI) of PS block were determined by GPC. The PDI of PS–PLLA was determined by GPC, and the numbers of L-LA repeating unit vs styrene repeating unit were determined by ^{1}H NMR analysis. The volume fraction of PLLA, f_{PLLA}^v, is calculated according to the assumption that the densities of PS and PLLA are 1.02 and 1.248 g/cm^3, respectively. The chemical characterization results for all PS–PLLA diblock coplymers are listed in Table 1.

Table 1. Characterization for Representative PS–PLLA Diblock Copolymers Synthesized

sample	$Mn^{PS a}$ (kg/mol)	$Mn^{PLLA b}$ (kg/mol)	PDI^a (M_w/M_n)	f_{PLLA}^v	phase[c]
PS98-PLLA49	10.2	7.0	1.15	0.35	gyroid
PS311-PLLA161	32.4	23.2	1.24	0.37	gyroid
PS433-PLLA204	45.0	29.4	1.17	0.35	gyroid
PS434-PLLA185	45.2	26.7	1.26	0.33	*Fddd*

[a]Mn^{PS} and polydispersity index (PDI) were determined by GPC. [b]Mn^{PLLA} was characterized by ^{1}H NMR. [c]Self-assembled phases were identified by TEM and SAXS results.

Sample Preparation. Bulk samples of PS–PLLA diblock copolymers were prepared by solution casting from dichloromethane (CH_2Cl_2) solution (10 wt % of PS–PLLA) at room temperature for 2 weeks and then dried in a vacuum oven at 65 °C for 3 days. The dried samples were first heated to the maximum annealing temperature, T_{max} = 180 °C, for 5 min to eliminate the PLLA crystalline residues that were formed during the preparation procedure. They were finally quenched to room temperature. After quenching from the microphase-separated ordered melt at 180 °C, the thermally treated block copolymers were sectioned using an ultramicrotome for TEM observation. Then, the PLLA blocks of the PS–PLLA bulk samples were removed by hydrolysis, using a 0.5 M basic solution that was prepared by dissolving 2 g of sodium hydroxide in a 40/60 (by volume) solution of methanol/water. After 3 days of hydrolysis, the

hydrolyzed samples were rinsed using a mixture of DI water and methanol and then used as templates for the following sol–gel reaction.

Sol–Gel Procedure. A SiO_2 precursor mixture was introduced into the PS templates by immersing the templates in TEOS/HCl(aq) (0.1 M)/methanol mixture (weight fraction of TEOS/HCl(aq) (0.1 M)/methanol = 10/1/25) with stirring at room temperature for 24 h and then treated under controlled humidity at 40 °C for 48 h. After drying, PS/SiO_2 nanohybrids were prepared;[10] then, the PS/SiO_2 nanohybrids were calcinated at 550 °C for enough time to remove PS matrix, and pure SiO_2 was formed.

Small-Angle X-ray (SAXS). Small-angle X-ray scattering (SAXS) experiments were conducted at the synchrotron X-ray beamline X27C at the National Synchrotron Radiation Research Center (NSRRC) in city of Hsinchu, Taiwan. The wavelength of the X-ray beam was 0.155 nm. A MAR CCD X-ray detector (MAR USA) was used to collect the two-dimensional (2D) SAXS patterns. A one-dimensional (1D) linear profile was obtained by integration of the 2D pattern. The scattering angle of the SAXS patter was calibrated using silver behenate, with the first-order scattering vector q* ($q* = 4\lambda^{-1} \sin \theta$, where 2θ is the scattering angle) being 1.076 nm^{-1}.

Transmission Electron Microscopy (TEM) and Electron Tomography (3D TEM). Bright-field TEM images were obtained using the mass–thickness contrast with a JEOL JEM-2100 LaB_6 transmission electron microscope (at an accelerating voltage of 200 kV). The PS/SiO_2 nanohybrids were sectioned by Leica Ultramicrotome (thickness ~ 150 nm) at room temperature for electron tomography. The microsections were collected on copper grids (100 mesh) covered by a polyvinyl formal membrane. For the requirement of image alignment to reconstruct 3D imaging, fiducial gold markers (diameter 10 nm, purchased from Polysciences, Inc.) were used and homogeneously distributed onto the microsections with the right amount of markers to observe self-assembled phase. Then, a series of 71 TEM projection images were collected from −70° to +70° tilt angles at an angular interval of 2° on a JEOL (JEM-2100) TEM operated at 200 kV. Images were recorded on a Gatan CCD camera. Alignment of the tilt series and 3D reconstruction were performed by using IMOD software. The reconstructed volume was then filtered by a 5 × 5 × 5 median filter for noise reduction. Analyze 4.0 (AnalyzeDirect) was then used to trim the filtered volume keeping only a volume of interest for further analysis. Finally, 3D analyses such as binarization, segmentation, and visualization of the volume of interest were achieved using Analyze 4.0.

Field-Emission Scanning Electron Microscopy (FESEM). FESEM observations were performed on a JEOL JSM-6700F using accelerating voltages of 1.5–3 keV. Before observations, the samples were sputter-coated with 2–3 nm of platinum to avoid the charge effect (the platinum coating thickness was estimated from a calculated deposition rate and experimental deposition time).

■ RESULTS AND DISCUSSION

Identification of Double Network Phases. Figure 1a shows the TEM micrograph of self-assembled PS98-PLLA49 from solution casting followed by quenching from microphase-separated melt after long-time thermal annealing. Network morphology can be clearly observed at which the PS matrix appears dark due to RuO_4 staining and the PLLA network appears bright. The projection image with wagon-wheel texture suggests the formation of a DG, and it is an image resulting from the [110] projection of the DG. Similar projection results can be found in self-assembled PS311-PLLA161 and PS433-PLLA204 as shown in Figures 1b and 1c, respectively. In contrast to the projection in Figure 1a, there is a significant increase in the dimensions of the DG for PS311-PLLA161 and PS433-PLLA204. As a result, the self-assembled phases of the PS–PLLA having different molecular weights and the volume fractions of PLLA near 0.35 are all identified as DG phases, and the results are in line with the phase behavior of PS–PLLA
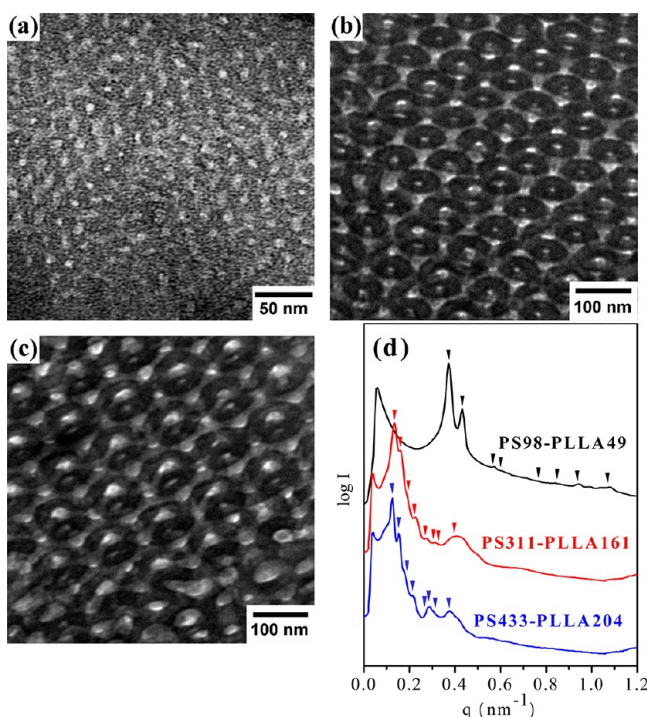
Figure 1. TEM micrographs of (a) PS98-PLLA49, (b) PS311-PLLA161, and (c) PS433-PLLA204 stained by RuO$_4$; (d) corresponding 1D SAXS profiles.

examined previously.[25] To further examine the forming DG phases, SAXS experiments were carried out, and one-dimensional (1D) SAXS profiles of those BCPs* are shown in Figure 1d. All of the scattering profiles show the reflections at (211), (220), (321), (400), (431), (440), (532), and (543) with the relative q values of $\sqrt{6}$, $\sqrt{8}$, $\sqrt{14}$, $\sqrt{16}$, $\sqrt{26}$, $\sqrt{32}$, $\sqrt{38}$, and $\sqrt{50}$ as marked by the triangles. Those SAXS results further confirm the formation of DG phase. On the basis of the primary peak, the d spacings of $(211)_{DG}$ plane for these three DG phases are determined as 16.9, 46.9, and 50.3 nm, respectively. Note that helical phase also appears in this composition range but will transform to DG phase after long-time thermal annealing. Here, those three PS−PLLA BCPs* were also thermally treated at 180 °C after solution casting for long enough annealing time to induce order−order phase transition from H* to DG, resulting in the formation of stable DG phase. As a result, a variety of stable DG phases with different dimensions can be fabricated in the self-assembly of the PS−PLLA BCPs*.

Identification of Single Network Phase. As described previously, various network phases such as DG, OBDD, and *Fddd* phases can be found in the self-assembly of diblock copolymers. Also, it is noted that the DG and OBDD phases are cubic structures whereas the *Fddd* phase is an orthorhombic structure. In contrast to the stable DG phase, the OBDD phase is identified as a metastable phase due to the inhomogeneous dispositions of the chain conformation for the constituted polymer chains.[28] For BCPs*, the chirality of the constituted chiral block is inevitable to play an important role on the molecular dispositions of the polymer chains in the micro-phase-separated domain. It is intuitive to expect the inhomogeneity in the chain conformations of the chiral block due to its higher persistent length, resulting in intermolecular chiral interaction to lower the Gibbs free energy of the self-

assembled morphology.[25] As a result, we speculate that stable network morphologies such as the OBDD might be found in the self-assembly of BCPs* by considering the formation of intrinsic inhomogeneity in the chain conformations of the chiral block (see below for details).

In contrast to the forming DG with the diffraction peaks at the relative q values of $\sqrt{6}$, $\sqrt{8}$, $\sqrt{14}$, $\sqrt{16}$, $\sqrt{26}$, $\sqrt{32}$, $\sqrt{38}$, and $\sqrt{50}$, interesting diffraction results can be found in a PS−PLLA BCP*, PS434-PLLA185, at which the diffraction peaks are identified at the relative q values of 1, 1.22, 1.55, 1.72, 1.95, 2.26, 2.75, and 2.93. On the basis of those reflections, one possible assignment is to refer them as the diffraction results from an OBDD phase.[14,15] Nevertheless, it is noted that the second characteristic peak of 1.22 can also appear in a *Fddd* phase.[17] Figure 2a shows the TEM micrograph of PS434-
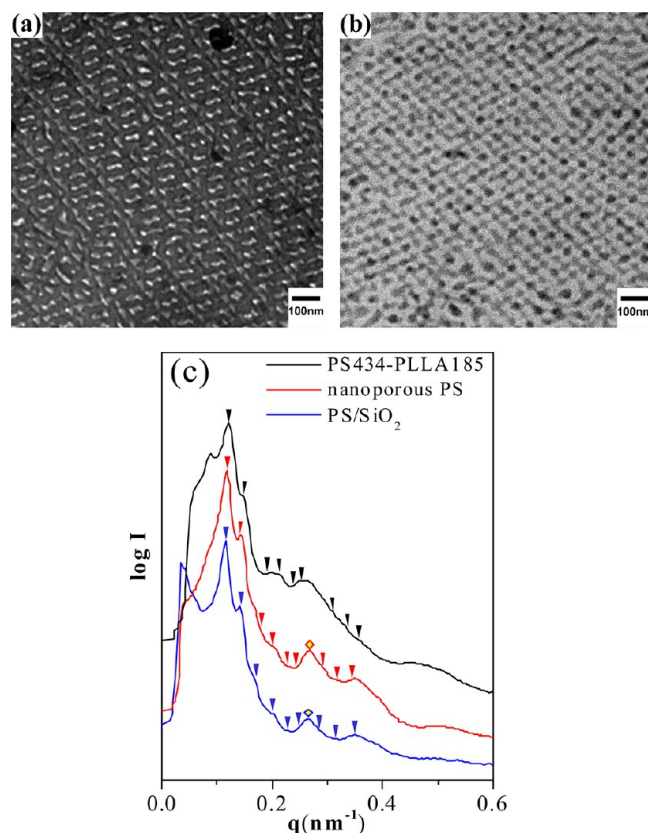

Figure 2. TEM micrographs of (a) PS434-PLLA185 stained by RuO$_4$ and (b) PS/SiO$_2$ nanohybrids from PS434-PLLA185 after PLLA hydrolysis followed by templated sol−gel reaction; (c) corresponding 1D SAXS profiles of PS434-PLLA185, nanoporous PS hydrolyzed from PS434-PLLA185 and PS/SiO$_2$ nanohybrids followed by templated sol−gel reaction.

PLLA185 at which unique projection with network-like texture can be found, suggesting the possible formation of a network phase. However, it is difficult to distinguish a network phase from projections using conventional 2D TEM. For instance, the projection results from DG and OBDD phases are also very similar to each other.[29] As a result, it is impractical to distinguish the OBDD and *Fddd* phases even with the combined SAXS and TEM results. As is known, the OBDD is a double network texture with tetravalent connectors whereas the *Fddd* is a single network texture with trivalent connectors.

Direct Visualization of Single Network Morphology.
To truly identify the forming phase, electron tomography (i.e.,
3D TEM) has been developed to directly visualize the self-
assembled phases of BCPs in real space.[26,30,31] By taking
advantage of the degradable character of polylactide, the self-
assembled phase after hydrolysis can be utilized to prepare a PS
template with nanochannels. Subsequently, sol−gel reaction
can be conducted within the nanochannels in the PS template
to fabricate nanohybrids.[32] Accordingly, in contrast to the
inaccessibility of the image reconstruction in RuO_4 stained PS−
PLLA samples, the PS/SiO_2 nanohybrids can be directly
visualized by TEM without RuO_4 staining because of a
significant increase in the mass−thickness contrast of the
SiO_2. Namely, a perfect sample with appropriate contrast for
image reconstruction through tomographic treatment can be
obtained by using hydrolyzed PS434-PLLA185 as a template
for the formation of PS/SiO_2 nanohybrids through sol−gel
reaction of TEOS.

On the basis of the primary peak at $q = 0.122$ nm^{-1} as shown
in Figure 2c, the interdomain spacing of the primary peak can
be calculated as 51.5 nm; the interdomain spacing of the
nanoporous PS was determined as 53.7 nm from the primary
peak at $q = 0.117$ nm^{-1}, indicating that there is a 4.2% variation
on its original size. Nevertheless, the SAXS peaks are all located
at q/q^* (q^* is the first-order peak) = 1, 1.22, 1.55, 1.72, 1.94,
2.00, 2.49, 2.75, and 2.93, indicating well preservation of the
microphase-separated structure after hydrolysis. Regarding the
changes in the shape and intensity of the SAXS profiles after
hydrolysis, we speculate that the changes are attributed to the
significant enhancement on the scattering contrast resulting
from the formation of air nanopores. Conversely, PS with well-
ordered nanochannels can be fabricated. Subsequently, the
nanoporous PS was treated as a template for sol−gel process to
create well-ordered PS/SiO_2 nanohybrids. Figure 2b shows the
projection image of the PS/SiO_2 microsection without RuO_4
staining. In contrast to Figure 2a, a similar projection image can
be observed, but the contrast is inversed. The inversed mass−
thickness contrast is attributed to the Z-contrast of Si which is
attributed to the formation of SiO_2.

Figure 2c also shows the corresponding 1D SAXS profiles of
the PS/SiO_2 nanohybrids. As compared to the result of the PS
template, the major diffraction peaks of the PS/SiO_2 nano-
hybrids at the relative q values of 1 and 1.22 remain unchanged,
reflecting the successful templating. The reconstructed 3D
image obtained by electron tomography and its digitally sliced
images are displayed in Figure 3. In the 3D image, the PS
microdomain is transparent for visual clarity so that the
network skeleton of the SiO_2 microdomain can be seen because
of significant mass−thickness contrast of the SiO_2. Unlike
OBDD, the SiO_2 microdomain is interconnected by a trivalent
node instead of tetravalent node. Most interestingly, a single
network structure as shown in Figure 3a can be clearly
identified, and it is very different to the DG network which
consists of two identical networks.[10,33] The projection from
Figure 3a will give similar image as seen from Figure 2b. One
repeated zone in the $x−y$ plane is marked as red rectangle in
Figure 3a. As shown in Figures 3b, the red rectangle zone is a
representative top view of an orthorhombic unit cell. The top
view is very similar to the simulated section where four
dispersed microdomains in a unit cell can be clearly recognized.
There are three arms diverged from every node as
demonstrated in the local texture as shown in Figures 3c and
3d. The "U" shape of the $Fddd$ unit cell can still be identified
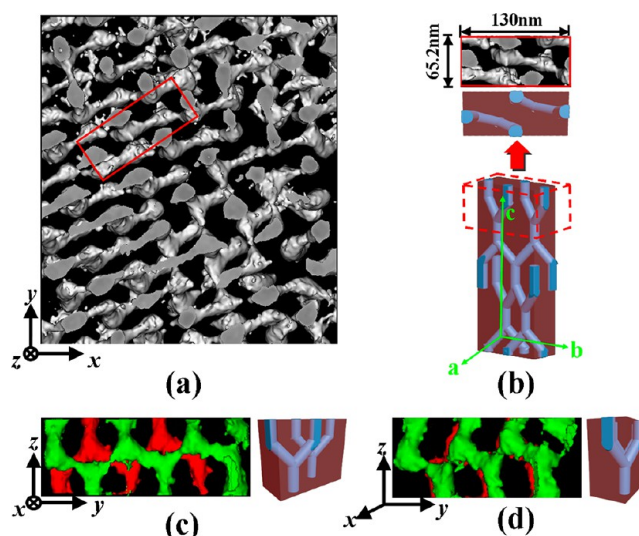

Figure 3. (a) 3D TEM of PS/SiO_2 from self-assembled PS434-
PLLA185 after hydrolysis followed by templated sol−gel reaction of
TEOS. The lattice constants of the unit cell in 3D image are $a = 65$ nm
and $b = 130$ nm; (b) the reconstructed $Fddd$ networks in the rectangle
red line box of (a); (c,d) side views of the reconstructed image from
different orientations.

and appear in crossed or overlapped images from different
orientations (Figures 3c and 3d) which shows a trivalent
connector. Accordingly, the obtained SiO_2 from self-assembled
PS434-PLLA185 after hydrolysis followed by templated
synthesis is truly a single network with trivalent connectors.
The nanostructured phase from the self-assembly of PS434-
PLLA185 is identified as an $Fddd$ phase instead of an OBDD
phase. As a result, the well-ordered $Fddd$ SiO_2 network in a PS
matrix can be clearly recognized in the PS/SiO_2 nanohybrids.
On the basis of the structure of $Fddd$ phase,[20] the a and b
dimensions can be determined as 65 and 130 nm according to
the 3D images. As a result, the observed network phase is a
representative of noncubic phase having the orthorhombic unit
cell so that the SAXS results of self-assembled PS−PLLA in
Figure 2c can be indexed as reflections of (111), (113), (131),
(133), (220), (222), (242), (313), and (315), corresponding to
the relative q values of 1, 1.22, 1.55, 1.72, 1.94, 2.00, 2.49, 2.75,
and 2.93 as marked by the triangles.[17] Also, the relatively strong
peak highlighted by a diamond might be attributed to the
overlapping of (222) and (242) reflections. On the basis of the
primary peak at $q = 0.122$ nm^{-1}, the interdomain spacing of
(111) of $Fddd$ phase, d_{111}, can be calculated as 51.5 nm; the d_{111}
of the nanoporous PS was determined as 53.7 nm from the
primary peak at $q = 0.117$ nm^{-1}. On the basis of the determined
$Fddd$ unit cell from the 3D TEM, the averaged lattice constants
of the orthorhombic unit cell can be finely calculated as $a =
62.5$ nm, $b = 125.6$ nm, and $c = 212.5$ nm from the
corresponding SAXS profile in Figure 2c, and the calculated
results are approximately in line with that from 3D TEM
observations. Interestingly, the value of the a:b:c ratio is very
close to 1:2:$2\sqrt{3}$, which coincides with the simulation results
for $Fddd$ phase by Morse and Ranjan.[22] Consequently, the
projection image in Figure 2a can be identified as a $[110]$
projection of the $Fddd$ phase, which is consistent with the
projection result from the $Fddd$ phases observed previously.[20]

Origin of $Fddd$ Formation. The PLLA volume fraction of
PS434-PLLA185 is 0.33, and this value is on the border of

0.33−0.37 composition region where the network phases are usually found. In contrast to theoretical prediction from Morse and Ranjan at which the forming *Fddd* phase should appear in weak segregation regime,[22] PS434-PLLA185 with a self-assembled *Fddd* structure is in a strong segregation region according to the determined χN.[25] The polymer chain with higher molecular weight would become a highly stretched chain as compared to the unperturbed end-to-end statistical length so as to amplify its packing frustration which prevents the stability of complex phases.[28] Note that PLLA is a chiral block and we found that PS−PLLA BCPs* can self-assemble into helical nanostructure due to the chirality effect of PLLA block on BCP self-assembly.[25] As calculated before, the persistent length of the chiral PLLA chain (11.9 Å) is larger than that of the racemic PLA chain (10.6 Å).[34a,35] The larger persistent length for the chiral PLLA chain is attributed to the formation of a helical chain conformation for a chiral polymer chain.[36] As a result, the longer persistent length of the PLLA helical chain conformation than that of the racemic polymer should be responsible for its lower packing energy. The χ values of the PS−PLLA BCPs* at 180 °C (0.13) is indeed higher than that of racemic PS−PLA (polystyrene-*b*-poly(D,L-lactide)) (0.10), indicating that the incompatibility between PS and chiral PLLA blocks is higher than that between PS and racemic PLA blocks.[25,34b] Namely, the chiral effect not only gives rise to the formation of helical chains (intramolecular effect) but also induces the formation of partially ordered microdomain (intermolecular interaction). The chiral PLLA chain with helical conformation and long persistent length would provide a specific geometrical property (i.e., helical steric hindrance) for self-assembly. The inhomogeneity in the chain conformations of the chiral block can be formed due to its higher persistent length so that the packing frustration can be alleviated. As a result, we speculate that stable network morphologies might be found in the self-assembly of BCPs* under strongly segregated condition by considering the formation of intrinsic inhomogeneity in the chain conformations of the chiral block. Consequently, it is possible to give the formation of a partially ordered state in the PLLA microdomains to reach a lower Gibbs free energy state due to the chiral intermolecular interaction. While self-assembled phase from BCP without the suggested chiral effect cannot be stable in the tripod center of *Fddd* due to the packing frustration, the intermolecular chiral interaction gives rise to lower the Gibbs free energy of the self-assembled morphology. These mutual interactions would allow PLLA blocks to generate local-ordered structures with packing of the helical segments. In this case, the entropic penalty correlated with chain stretching or packing frustration can be balanced by the release of free energy on forming the partially ordered regions in the microdomains due to the chirality of the constituted chiral PLLA block that facilitates the stable *Fddd* formation at strong segregation regime.[15]

Optical Properties of *Fddd*. *Fddd* network is an orthorhombic unit cell (namely, a noncubic structure with anisotropic unit cell) which may result in unique crystallographic optical axes. Light gets polarized when transmitted through a structured liquid containing such optical anisotropy. Hence, noncubic structures are birefringent objects, and transmitted light intensity will get recorded at the detector in the polarized light microscope experiment. By contrast, cubic ordered morphologies do not have any unique crystallographic optical axis and hence do not show birefringence. Disordered states in block copolymers have concentration fluctuations that

are random in nature with no preferred spatial orientation and hence are nonbirefringent. For both cubic states and disordered states, the detector will measure zero transmitted light intensity. The OBDD and DG structures are all cubic phases at which the OBDD exhibit the characteristic diffraction peaks with the relative q values of $\sqrt{2}:\sqrt{3}:\sqrt{4}:\sqrt{6}:\sqrt{8}$ from SAXS results, and the results of DG give the relative q values of $\sqrt{6}:\sqrt{8}:\sqrt{14}:\sqrt{16}:\sqrt{20}$.[15] By contrast, the *Fddd* is a noncubic phase, and the characteristic diffraction peaks with the relative q values of 1:1.22:1.55:1.72:1.81:1.95:2.00 can be found.[17] Therefore, it is reasonable to expect an optical birefringence from the sample with *Fddd* phase while the samples with the OBDD and DG phases are nonbirefringent materials. As shown in Figure 4, there is an obvious color contrast at two orthogonal
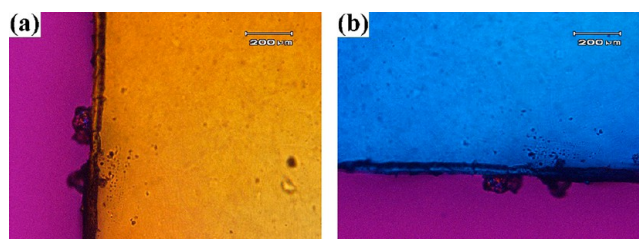

Figure 4. Observation of PS434-PLLA185 bulk by PLM between crossed polarizers passing through the bulk after introducing a gypsum plate. The gypsum plate is inserted into the polarized light microscopy in the 45° position.

directions in PLM images for PS434-PLLA185, a *Fddd* phase, due to optical anisotropy (i.e., birefringence). By contrast, the birefringence of the BCPs* with DG examined is insignificant under PLM (Figures 5a−d). The birefringence may arise from the anisotropic orientation of polymeric chains (i.e., intrinsic birefringence)[37] or from the noncubic texture of structure (i.e., the form birefringence).[38] For PS/SiO$_2$ nanohybrids from templating of hydrolyzed PS434-PLLA185, the birefringence remains (Figures 5e,f). As a result, the birefringence should mainly arise from the noncubic texture of structure (i.e., form birefringence) instead of the anisotropy of polymer chain (i.e., intrinsic birefringence). This approach might give an easy way to identify the anisotropic phase. The birefringent materials might give potential application in optoelectronics industry.[39]

Nanoporous DG and *Fddd* SiO$_2$. It is also noted that nanoporous SiO$_2$ with *Fddd* structure can be fabricated by using the PS/SiO$_2$ nanohybrids as a template for calcination. As shown in Figure 6a, after high-temperature thermal treatment, the free-standing, well-ordered porous SiO$_2$ with network texture can be clearly visualized due to the degeneration of the PS matrix after calcination. A single network can be clearly seen which implies that it is indeed an *Fddd* phase. The domain size of the SiO$_2$ network is about 24 nm on average while the domain size of the SiO$_2$ network in Figure 2b is about 30 nm. We speculate that the change of domain size results from the calcination, leading to a decrease in proportional dimension of the *Fddd* feature over high-temperature treatment. Nevertheless, in contrast to the nanoporous DG SiO$_2$ obtained from the same manufacturing process, there is least problem for the preservation of original network. Note that a DG structure is composed of a matrix and a pair of interpenetrating but independent single-gyroid (SG) networks. Consequently, significant displacement of these two SiO$_2$ networks will occur after removal of the PS matrix because these two
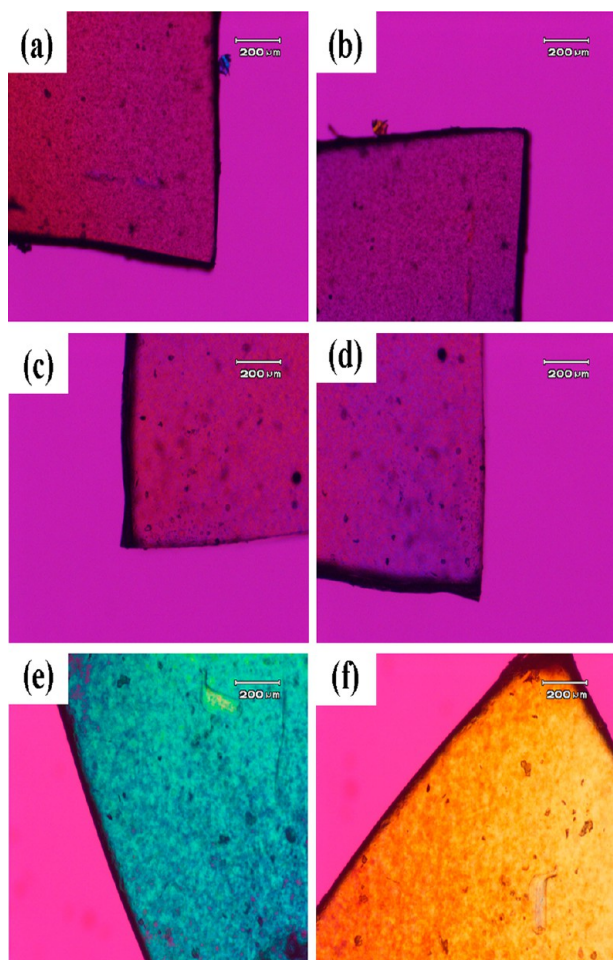
Figure 5. PLM images at two orthogonal directions of (a, b) PS311-PLLA161 bulk, (c, d) PS433-PLLA204 bulk, and (e, f) PS/SiO$_2$ nanohybrid from PS434-PLLA185 templating.
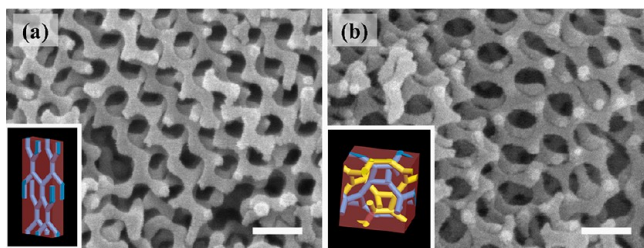

Figure 6. FESEM micrograph of nanoporous SiO$_2$ with (a) *Fddd* and (b) DG structures from calcination of PS/SiO$_2$ after high-temperature thermal treatment. The DG-forming PS template is obtained by using hydrolyzed PS433-PLLA204 as a template. Insets show the illustrations of the networks. The scale bar corresponds to 100 nm length.

independent robust SG-forming SiO$_2$ networks will be suspended and further displaced for stability consideration.[10] As a result, the character of the single network of *Fddd* structure can be further confirmed.

To demonstrate the advantage of using the *Fddd*-forming nanoporous SiO$_2$ for applications, the analyses of the specific surface area and the porosity of the nanoporous SiO$_2$ were determined by measuring the N$_2$ adsorption−desorption isotherm. Figure 7 shows a combination of typical type I and type IV isotherms (BDDT classification). In the range of low
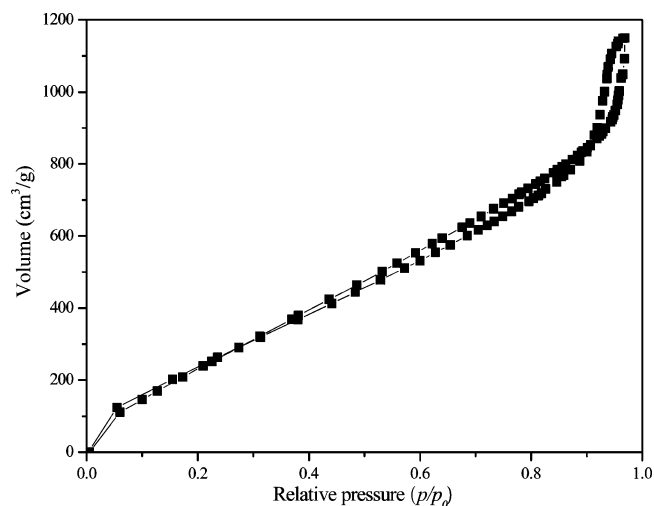

Figure 7. N$_2$ adsorption−desorption isotherm of nanoporous *Fddd* SiO$_2$.

relative pressure (below 0.3), the isotherm exhibits a typical type I isotherm. We speculate that the high adsorption of the type I isotherm is attributed to the formation of the micropores resulting from the evaporation of solvent from sol−gel reaction as described in the Experimental Section. Also, the curve exhibits two hysteresis loops in the high relative pressure region from 0.4 to 1 (type IV isotherms), indicating bimodal pore-size distribution. The hysteresis loop in the relative pressure between 0.9 and 1.0 is close to a type H1 in which both the adsorption−desorption branches are nearly vertical and they are also parallel to each other, indicating that the nanoporous SiO$_2$ possesses ordered texture with uniform pores. The relative pressure hysteresis loop between 0.4 and 0.9 can be referred to type H2, suggesting the existence of randomly distributed nanopores with smaller average pore size due to the deformation and collapse of the nanopores after calcination. The specific surface area and the porosity of the nanoporous SiO$_2$ determined by BET are 1170 m^2/g and 69%, respectively. In contrast to the nanoporous *Fddd* SiO$_2$, the porosity of the nanoporous DG-forming SiO$_2$ is about 66% from nitrogen adsorption experiments, and the specific surface area is calculated as 790 m^2/g.[10] By virtue of the network structure, this nanoporous *Fddd* SiO$_2$ with extremely high specific surface area and high porosity is a potential candidate for devices which need large surface area or a solid skeleton structure used in such as catalyst,[3] photovoltaic industry,[8−10] separation,[40] and sensor.[41]

■ CONCLUSIONS

In summary, an *Fddd* phase in a chiral block copolymer, PS−PLLA with PLLA volume fraction 0.33, was identified. The 3D TEM images clearly show that this phase appears as a 3-fold single network. Its lattice constants of unit cell can be calculated from 3D TEM and SAXS, respectively. These two lattice constant results are both consistent with the theoretical ratio $a{:}b{:}c = 1{:}2{:}2\sqrt{3}$, which illustrates the noncubic structure. The PLM image demonstrates the anisotropic character of the *Fddd* phase. Nanoporous *Fddd* SiO$_2$ with free-standing character can be fabricated by using the *Fddd* phase as a template for sol−gel reaction to give well-ordered nanoporous ceramics. In contrast to the nanoporous DG SiO$_2$, the nanoporous *Fddd* SiO$_2$

possesses much higher specific surface area with less concerns of structure collapse during calcination.

■ AUTHOR INFORMATION

Corresponding Author

*Tel 886-3-5738349; Fax 886-3-5715408; e-mail rmho@mx. nthu.edu.tw.

Notes

The authors declare no competing financial interest.

■ REFERENCES

(1) Matsen, M. W.; Bates, F. S. Unifying Weak- and Strong-Segregation Block Copolymer Theories. *Macromolecules* **1996**, *29*, 1091−1098.

(2) Bates, F. S.; Fredrickson, G. H. Block Copolymer Thermodynamics: Theory and Experiment. *Annu. Rev. Phys. Chem.* **1990**, *41*, 525−557.

(3) Hsueh, H. Y.; Ho, R. M. Bicontinuous Ceramics with High Surface Area from Block Copolymer Templates. *Langmuir* **2012**, *28*, 8518−8529.

(4) Wu, D. C.; Nese, A.; Pietrasik, J.; Liang, Y. R.; He, H. K.; Kruk, M.; Huang, L.; Kowalewski, T.; Matyjaszewski, K. Preparation of Polymeric Nanoscale Networks from Cylindrical Molecular Bottlebrushes. *ACS Nano* **2012**, *6*, 6208−6214.

(5) Hsueh, H. Y.; Huang, Y. C.; Ho, R. M.; Lai, C. H.; Makida, T.; Hasegawa, H. Nanoporous Gyroid Nickel from Block Copolymer Templates via Electroless Plating. *Adv. Mater.* **2011**, *23*, 3041−3046.

(6) Finnemore, A. S.; Scherer, M. R. J.; Langford, R.; Mahajan, S.; Ludwigs, S.; Meldrum, F. C.; Steiner, U. Nanostructured Calcite Single Crystals with Gyroid Morphologies. *Adv. Mater.* **2009**, *21*, 3928−3932.

(7) Scherer, M. R. J.; Li, L.; Cunha, P. M. S.; Scherman, O. A.; Steiner, U. Enhanced Electrochromism in Gyroid-Structured Vanadium Pentoxide. *Adv. Mater.* **2012**, *24*, 1217−1221.

(8) Urbas, A. M.; Maldovan, M.; DeRege, P.; Thomas, E. L. Bicontinuous Cubic Block Copolymer Photonic Crystals. *Adv. Mater.* **2002**, *14*, 1850−1853.

(9) Crossland, E. J. W.; Kamperman, M.; Nedelcu, M.; Ducati, C.; Wiesner, U.; Smilgies, D.; Toombes, G. E. S.; Hillmyer, M. A.; Ludwigs, S.; Steiner, U.; Snaith, H. J. A Bicontinuous Double Gyroid Hybrid Solar Cell. *Nano Lett.* **2009**, *9*, 2807−2812.

(10) Hsueh, H. Y.; Chen, H. Y.; She, M. S.; Chen, C. K.; Ho, R. M.; Gwo, S.; Hasegawa, H.; Thomas, E. L. Inorganic Gyroid with Exceptionally Low Refractive Index from Block Copolymer Templating. *Nano Lett.* **2010**, *10*, 4994−5000.

(11) Schulz, M. F.; Bates, F. S.; Almdal, K.; Mortensen, K. Epitaxial Relationship for Hexagonal-to-Cubic Phase-Transition in a Block-Copolymer Mixture. *Phys. Rev. Lett.* **1994**, *73*, 86−89.

(12) Hajduk, D. A.; Harper, P. E.; Gruner, S. M.; Honeker, C. C.; Kim, G.; Thomas, E. L.; Fetters, L. J. The Gyroid: A New Equilibrium Morphology in Weakly Segregated Diblock Copolymers. *Macromolecules* **1994**, *27*, 4063−4075.

(13) Matsen, M. W.; Schick, M. Stable and Unstable Phases of a Diblock Copolymer Melt. *Phys. Rev. Lett.* **1994**, *72*, 2660−2663.

(14) Winey, K. I.; Thomas, E. L.; Fetters, L. J. The Ordered Bicontinuous Double-Diamond Morphology in Diblock Copolymer/Homopolymer Blends. *Macromolecules* **1992**, *25*, 422−428.

(15) Chu, C. Y.; Lin, W. F.; Tsai, J. C.; Lai, C. S.; Lo, S. C.; Chen, H. L.; Hashimoto, T. Order-Order Transition between Equilibrium Ordered Bicontinuous Nanostructures of Double Diamond and Double Gyroid in Stereoregular Block Copolymer. *Macromolecules* **2012**, *45*, 2471−2477.

(16) Tyler, C. A.; Morse, D. C. Orthorhombic *Fddd* Network in Triblock and Diblock Copolymer Melts. *Phys. Rev. Lett.* **2005**, *94*, 208302/1−208302/4.

(17) Takenaka, M.; Wakada, T.; Akasaka, S.; Nishitsuji, S.; Saijo, K.; Shimizu, H.; Kim, M. I.; Hasegawa, H. Orthorhombic *Fddd* Network in Diblock Copolymer Melts. *Macromolecules* **2007**, *40*, 4399−4402.

(18) Yamada, K.; Nonomura, M.; Ohta, T. Kinetics of Morphological Transitions in Microphase-Separated Diblock Copolymers. *Macromolecules* **2004**, *42*, 5762−5777.

(19) Jung, J.; Park, H. W.; Lee, J. Y.; Huang, H. Y.; Chang, T. H.; Rho, Y. C.; Ree, M. H.; Sugimori, H.; Jinnai, H. Structural Characterization of the *Fddd* Phase in a Diblock Copolymer Thin Film by Electron Microtomography. *Soft Matter* **2011**, *7*, 10424−10428.

(20) Bailey, T. S.; Hardy, C. M.; Epps, T. H., III; Bates, F. S. A Noncubic Triply Periodic Network Morphology in Poly(isoprene-b-styrene-b-ethylene oxide) Triblock Copolymers. *Macromolecules* **2002**, *35*, 7007−7017.

(21) Yamada, K.; Nonomura, M.; Ohta, T. *Fddd* Strcture in AB-type Diblock Copolymers. *J. Phys.: Condens. Matter.* **2006**, *18*, L421−L427.

(22) Ranjan, A.; Morse, D. C. Landau Theory of the Orthorhombic *Fddd* Phase. *Phys. Rev. E* **2006**, *74*, 011803−011803.

(23) Ho, R. M.; Chiang, Y. W.; Tsai, C. C.; Lin, C. C.; Ko, B. T.; Huang, B. H. Three-Dimensionally Packed Nanohelical Phase in Chiral Block Copolymers. *J. Am. Chem. Soc.* **2004**, *126*, 2704−2705.

(24) Ho, R. M.; Chiang, Y. W.; Lin, S. C.; Chen, C. K. Helical Architectures from Self-Assembly of Chiral Polymers and Block Copolymers. *Prog. Polym. Sci.* **2011**, *36*, 376−453.

(25) Ho, R. M.; Chiang, Y. W.; Chen, C. K.; Wang, H. W.; Hasegawa, H.; Akasaka, S.; Thomas, E. L.; Burger, C.; Hsiao, B. S. Block Copolymers with a Twist. *J. Am. Chem. Soc.* **2009**, *131*, 18533−18542.

(26) Chen, C. K.; Hsueh, H. Y.; Chiang, Y. W.; Ho, R. M.; Akasaka, S.; Hasegawa, H. Single Helix to Double Gyroid in Chiral Block Copolymers. *Macromolecules* **2010**, *43*, 8637−8644.

(27) Ho, R. M.; Li, M. C.; Lin, S. C.; Wang, H. F.; Lee, Y. D.; Hasegawa, H.; Thomas, E. L. Transfer of Chirality from Molecule to Phase in Self-Assembled Chiral Block Copolymers. *J. Am. Chem. Soc.* **2012**, *134*, 10974−10986.

(28) Matsen, M. W.; Bates, F. S. Origins of Complex Self-Assembly in Block Copolymers. *Macromolecules* **1996**, *29*, 7641−7644.

(29) Meuler, A. J.; Hillmyer, M. A.; Bates, F. S. Ordered Network Mesostructures in Block Polymer Materials. *Macromolecules* **2009**, *42*, 7221−7250.

(30) Mareau, V. H.; Akasaka, S.; Osaka, T.; Hasegawa, H. Direct Visualization of the Perforated Layer/Gyroid Grain Boundary in a Polystyrene-*block*-polyisoprene/Polystyrene Blend by Electron Tomography. *Macromolecules* **2007**, *40*, 9032−9039.

(31) Jung, J.; Park, H. W.; Lee, S.; Lee, H.; Chang, T.; Matsunaga, K.; Jinnai, H. Effect of Film Thickness on the Phase Behaviors of Diblock Copolymer Thin Film. *ACS Nano* **2010**, *4*, 3109−3116.

(32) Tseng, W. H.; Chen, C. K.; Chiang, Y. W.; Ho, R. M.; Akasaka, S.; Hasegawa, H. Helical Nanocomposites from Chiral Block Copolymer Templates. *J. Am. Chem. Soc.* **2009**, *131*, 1356−1357.

(33) Park, H. W.; Jung, J.; Chang, T.; Matsunaga, K.; Jinnai, H. New Epitaxial Phase Transition between DG and HEX in PS-*b*-PI. *J. Am. Chem. Soc.* **2009**, *131*, 46−47.

(34) (a) Anderson, K. S.; Hillmyer, M. A. Melt Chain Dimensions of Polylactide. *Macromolecules* **2004**, *37*, 1857−1862. (b) Zalusky, A. S.; Olayo-Valles, R.; Wolf, J. H.; Hillmyer, M. A. Ordered Nanoporous Polymers from Polystyrene-Polylactide Block Copolymers. *J. Am. Chem. Soc.* **2002**, *124*, 12761−12773.

(35) Joziasse, C. A. P.; Veenstra, H.; Grijpma, D. W.; Pennings, A. J. On the Chain Stiffness of Poly(lactide)s. *Macromol. Chem. Phys.* **1996**, *197*, 2219−2229.

(36) Grosberg, A. Y.; Khokhlov, A. R. *Statistical Physics of Macromolecules*; AIP: New York, 1994; pp 289−336.

(37) (a) Lodge, T. P.; Fredrickson, G. H. *Macromolecules* **1992**, *25*, 5643−5650. (b) Li, M. C.; Chang, G. W.; Lin, T.; Ho, R. M.; Chuang, W. T.; Kooi, S. Birefringence Control of Semicrystalline Block Copolymers by Crystallization under Confinement. *Langmuir* **2010**, *26*, 17640−17648.

(38) (a) Mita, K.; Takenaka, M.; Hasegawa, H.; Hashimoto, T. Cylindrical Domains of Block Copolymers Developed via Ordering under Moving Temperature Gradient: Real-Space Analysis. *Macromolecules* **2008**, *41*, 8789−8799. (b) Hashimoto, T.; Shibayama, M.; Kawai, H.; Meier, D. J. Confined-Chain Statistics of Block Polymers and Estimation of Optical Anisotropy and Domain Size. *Macromolecules* **1985**, *18*, 1855−1864.

(39) Forster, J. D.; Park, J. G.; Mittal, M.; Noh, H.; Schreck, C. F.; O'Hern, C. S.; Cao, H.; Furst, E. M.; Dufresne, E. R. Assembly of Optical-Scale Dumbbells into Dense Photonic Crystals. *ACS Nano* **2011**, *5*, 6695−6700.

(40) Davis, M. E. Ordered Porous Materials for Emerging Applications. *Nature* **2002**, *417*, 813−821.

(41) de la Escosura-Muñiz, A.; Merkoçi, A. Nanochannels Preparation and Application in Biosensing. *ACS Nano* **2012**, *6*, 7556−7583.